

Edge-of-chaos enhanced quantum-inspired algorithm for combinatorial optimization

Hayato Goto^{1,2}, Ryo Hidaka¹, Kosuke Tatsumura¹

¹*Corporate Laboratory, Toshiba Corporation, Kawasaki, Kanagawa 212-8582, Japan*

²*RIKEN Center for Quantum Computing (RQC), Wako, Saitama 351-0198, Japan*

(Dated: December 24, 2025)

Nonlinear dynamical systems with continuous variables can be used for solving combinatorial optimization problems with discrete variables. Numerical simulations of them are also useful as heuristic algorithms with a desirable property, namely, parallelizability, which allows us to execute them in a massively parallel manner, leading to ultrafast performance. However, the dynamical-system approaches with continuous variables are usually less accurate than conventional approaches with discrete variables such as simulated annealing. To improve the solution accuracy of a quantum-inspired algorithm called simulated bifurcation (SB), which was found from classical simulation of a quantum nonlinear oscillator network exhibiting quantum bifurcation, here we generalize it by introducing nonlinear control of individual bifurcation parameters and show that the generalized SB (GSB) can achieve surprisingly high performance, namely, almost 100% success probabilities for some large-scale problems. As a result, the time to solution for a 2,000-variable problem is shortened to 10 ms by a GSB-based machine, which is two orders of magnitude shorter than the best known value, 1.3 s, previously obtained by an SB-based machine. To examine the reason for the ultrahigh performance, we investigated chaos in the GSB changing the nonlinear-control strength and found that the dramatic increase of success probabilities happens near the edge of chaos. That is, the GSB can find a solution with high probability by harnessing the edge of chaos. This finding suggests that dynamical-system approaches to combinatorial optimization will be enhanced by harnessing the edge of chaos, opening a broad possibility to tackle intractable combinatorial optimization problems by physics-inspired approaches.

I. INTRODUCTION

Selecting the best option among many candidates is important for making industrial and social activities more efficient. The mathematical formulation of this often results in a so-called combinatorial optimization problem with discrete variables such as bits. Unfortunately, such a problem is notoriously hard because of the exponentially large number of solution candidates with respect to the problem size, which is called combinatorial explosion [1]. To tackle such intractable problems, special-purpose machines [2], especially so-called Ising machines [3], have recently attracted much attention. A major approach to such machines is based on nonlinear dynamical systems [3–48], such as neural networks [4, 5], nonlinear optical oscillator networks [6–11], and nonlinear quantum oscillator networks [12–17]. In addition to real physical systems, numerical simulations of them are also useful as heuristic algorithms for combinatorial optimization [4, 5, 18–35]. Unlike classical systems such as neural networks and optical oscillator networks, quantum oscillator networks cannot be simulated efficiently, because they are enough to realize universal quantum computation [49, 50], which is believed not to be simulated efficiently by classical computers [51]. Thus, simulating a classical counterpart (classical Hamiltonian system [52–54]) of a quantum oscillator network exhibiting quantum bifurcation has been proposed, which is called simulated bifurcation (SB) [22–28]. Notably, the dynamical system-based algorithms usually have a desirable property: parallelizability. That is, we can execute the algorithms in a massively parallel manner, unlike a representative algorithm called simulated annealing (SA) [1, 55], leading

to ultrafast performance by using cutting-edge many-core processors, such as graphics processing units (GPUs) and field-programmable gate arrays (FPGAs). However, the dynamical system-based algorithms with continuous variables are usually less accurate than conventional discrete-variable algorithms such as SA.

In this work, we focus on the SB and propose a new method for improving its solution accuracy. Because of its parallelizability and high solution accuracy, the SB has demonstrated ultrafast performance using GPUs and FPGAs [22–26], and hence it is one of the most promising dynamical system-based algorithms. There are three major variants of SB: adiabatic SB (aSB) based on classical adiabatic evolution [22], ballistic SB (bSB) obtained from aSB by replacing nonlinear potential walls with perfectly inelastic infinite walls [24], and discrete SB (dSB) obtained from bSB by discretizing continuous variables via the sign function [24]. Note that all the SBs have a single bifurcation parameter controlling bifurcations of all the SB variables, which is usually scheduled deterministically, e.g., linearly with respect to time. The bSB can find good approximate solutions the fastest but cannot find best known solutions for large-scale problems [24]. The dSB was introduced to improve the accuracy of the bSB and succeeded in finding the best known solutions [24].

Toward further improvement, here we generalize the bSB by introducing nonlinear control of individual bifurcation parameters corresponding to the bSB variables, which we call the generalized bSB (GbSB). Surprisingly, the GbSB can find the best known solutions with much higher probabilities, sometimes almost 100%, for some large-scale problems than the dSB. Also importantly, the GbSB maintains the advantage of the SB, namely, par-

allelizability. To demonstrate it, we implemented the GbSB with an FPGA in a massively parallel manner and achieved one or two orders of magnitude shorter times to solution for large-scale problems than a previous dSB-based FPGA machine [24]. To examine the reason for the ultrahigh performance of the GbSB, we investigated chaos [56, 57] in the GbSB changing the nonlinear-control strength. As is well known as the butterfly effect, the chaos causes a large difference between two trajectories with very close initial conditions due to nonlinearity. We actually observed that such two trajectories result in completely different states at the final time in the GbSB when the nonlinear-control strength is sufficiently large, clearly suggesting the chaos. Most importantly, we found that the dramatic increase of the success probabilities occurs near the edge of chaos in terms of the nonlinear-control strength. The edge-of-chaos effect has been known well in the field of artificial intelligence [58–63], but not well for combinatorial optimization [64–66]. Thus, we expect that the SB enhanced by harnessing the edge of chaos will open a broad possibility for dynamical-system approaches to combinatorial optimization.

II. GENERALIZED BALLISTIC SIMULATED BIFURCATION (GBSB)

In this work, we focus on the Ising problem, the target problem of Ising machines [3], defined by the following objective (cost) function:

$$E_{\text{Ising}} = -\frac{1}{2} \sum_{i=1}^N \sum_{j=1}^N J_{i,j} s_i s_j, \quad (1)$$

where s_i denotes the i th Ising spin taking 1 or -1 , N is the number of the spins, $J_{i,j}$ is the interaction coefficient between the i th and j th spins ($J_{i,j} = J_{j,i}$ and $J_{i,i} = 0$), and E_{Ising} denotes the energy of the Ising model. The Ising problem is to find a spin configuration minimizing the Ising energy. This problem is known as an NP-hard problem [51, 67], and hence many other problems can be reduced to this problem with only polynomial overheads [68]. To solve the Ising problem, the bSB numerically simulates the classical Hamiltonian dynamics with the following time-dependent Hamiltonian for N oscillators:

$$H_{\text{bSB}}(t) = \frac{1}{2} \sum_{i=1}^N y_i^2 + \frac{p(t)}{2} \sum_{i=1}^N x_i^2 - \frac{c}{2} \sum_{i=1}^N \sum_{j=1}^N J_{i,j} x_i x_j, \quad (2)$$

where x_i and y_i are the position and momentum, respectively, of the i th oscillator corresponding to the i th spin s_i via $s_i = \text{sgn}(x_i)$, $p(t)$ is a bifurcation parameter that varies from 1 to 0, and c is a constant to tune the first bifurcation point [22, 24]. To confine the positions within a finite range, we also introduce perfectly inelastic infinite

walls at $x_i = \pm 1$. More explicitly, the bSB is defined by the following update rules:

$$y_i(t_{m+1}) = y_i(t_m) - \frac{\partial H_{\text{bSB}}}{\partial x_i} \Delta_t$$

$$= y_i(t_m) - \left[p(t_{m+1}) x_i(t_m) - c \sum_{j=1}^N J_{i,j} x_j(t_m) \right] \Delta_t, \quad (3)$$

$$x_i(t_{m+1}) = x_i(t_m) + \frac{\partial H_{\text{bSB}}}{\partial y_i} \Delta_t = x_i(t_m) + y_i(t_{m+1}) \Delta_t, \quad (4)$$

$$\text{If } |x_i(t_{k+1})| > 1, \text{ then } x_i(t_{k+1}) \leftarrow \text{sgn}[x_i(t_{m+1})]$$

$$\text{and } y_i(t_{m+1}) = 0, \quad (5)$$

where Δ_t is a time step and $t_m = \Delta_t m$ ($m = 0, 1, \dots, M$) is the discrete time (t_M is the final time of the simulation). Note that the update rules given by Eqs. (3) and (4) are based on the numerical integration method called the symplectic Euler method [52], and Eq. (5) describes the above-mentioned walls at $x_i = \pm 1$. Importantly, we can update all x_i (all y_i) simultaneously according to Eq. (4) [Eq. (3)]. This is the parallelizability of the SB allowing for ultrafast performance [22–26]. [Note that the processing for the walls in Eq. (5) is also parallelizable.] The bSB has a single bifurcation parameter $p(t)$, which is usually scheduled linearly from 1 to 0 as $p(t_m) = 1 - m/M$ or equivalently

$$p(t_{m+1}) = p(t_m) - \frac{1}{M} = p(t_m) - \frac{p(t_m)}{M - m} \quad (6)$$

with $p(0) = 1$. We generalize the bSB by introducing individual bifurcation parameters $p_i(t)$ corresponding to x_i [$p(t_{m+1})$ in Eq. (3) is replaced by $p_i(t_{m+1})$] and controlling them by

$$p_i(t_{m+1}) = p_i(t_m) - [1 - A x_i^2(t_m)] \frac{p_i(t_m)}{M - m}, \quad (7)$$

where A is a constant determining the strength of the nonlinear control of $p_i(t)$. When A equals zero, the GbSB becomes the conventional bSB.

The meaning of Eq. (7) is as follows. After a bifurcation, each oscillator approaches a wall, and consequently some of the oscillators stick to the walls in the middle of searching for a solution, resulting in trapping at a local minimum of the Hamiltonian (potential) with the walls. This is the reason why the conventional bSB usually results in only an approximate solution and cannot find an optimal one. To avoid sticking to the walls, the nonlinear control of $p_i(t)$ in Eq. (7) reduces the decreasing rate of $p_i(t)$ for the oscillator close to a wall. Thus the individual bifurcation parameters are automatically controlled such that the oscillators do not stick to the walls, leading to higher solution accuracy by avoiding trapping at local minima. As shown below, this control leads to dramatic increase of the success probabilities of finding best known solutions for large-scale problems.

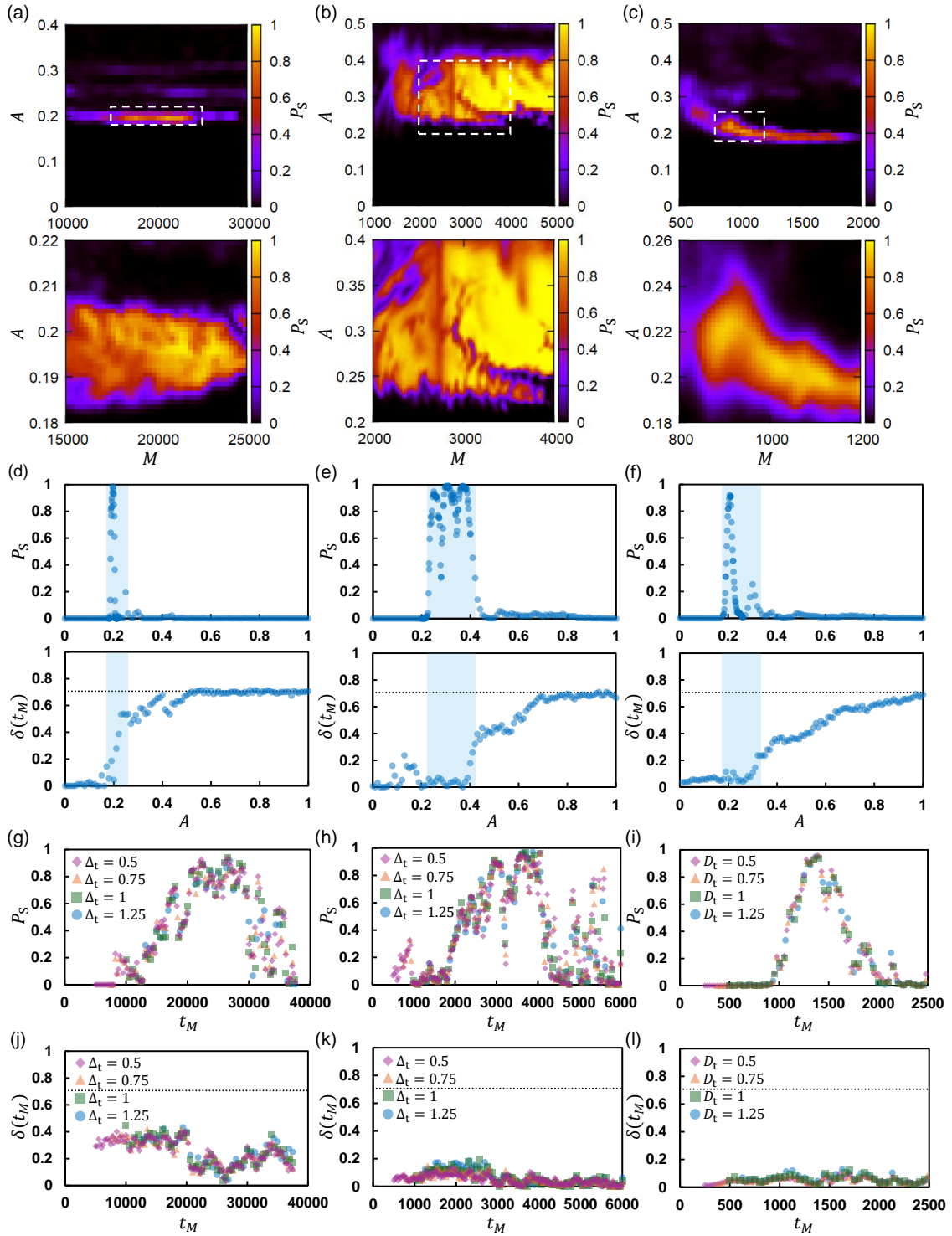


FIG. 1. Numerical results of the GbSB. (a) Success probability, P_S , of finding the best known cut value of K_{2000} by the GbSB with $\Delta_t = 1.25$ and various values of M and A . See Appendix A for the setting of c . The lower figure is the enlargement of the part enclosed by the dashed rectangle in the upper figure. P_S was evaluated by 1,000 times repetition with different initial conditions. (b) and (c) Results corresponding to (a) for an instance of the 700-spin Ising problem and G6, respectively. The time step is set as $\Delta_t = 1.25$ and $D_t = 1.25$ [see Eq. (A4) in Appendix A], respectively. See Appendix A for the setting of c . (d) P_S in a (upper figure) and normalized distance, $\delta(t_M)$, at the final time (lower figure) for K_{2000} when $M = 21,500$ in (a). $\delta(t_M)$ was evaluated by averaging 100 results with different initial conditions. The regions highlighted in blue show the condition that P_S becomes particularly high. The dotted line in the lower figure shows $\delta(t_M) = 1/\sqrt{2}$, which indicates chaos. (e) and (f) Results corresponding to (d) for the 700-spin instance when $M = 3,000$ in (b) and G6 when $M = 1,000$ in (c), respectively. (g-i) P_S for K_{2000} , the 700-spin instance, and G6, respectively, for different values of the time step Δ_t and different final times $t_M = \Delta_t M$. A was set to 0.2, 0.25, and 0.2, respectively. (j-l) $\delta(t_M)$ corresponding to (g-i), respectively.

III. PERFORMANCE OF THE GBSB

To evaluate the performance of the GbSB, we first solved a standard benchmark problem named K_{2000} , a 2,000-node MAX-CUT problem [51] equivalent to a 2,000-spin Ising problem with all-to-all connectivity ($J_{i,j} \in \{\pm 1\}$) [8, 20, 22, 24, 27, 35]. In this work, we evaluate the cut value only at the final time, because its calculation is time-consuming. (We confirmed that the present results remain unchanged even if we evaluate the cut value at all the time steps and select the best one.) The best known cut value of K_{2000} is 33,337 reported in ref. 24. Figure 1(a) shows the success probability, P_S , of finding the best known value by the GbSB with various values of M and A . [See Appendix A for the detailed settings of the other parameters. Also see Appendix B for average cut values corresponding to Figs. 1(a-c).] It thus turns out that the GbSB with appropriate values of M and A can find the best known value of K_{2000} with almost 100% probability. To the best of our knowledge, this is the highest success probability of this problem. (In Fig. 1(b), we can see a vertical stripe around $M = 2700$ where P_S becomes relatively low. This is not an artifact but its underlying cause is difficult to explain. This may be a unique circumstance of this instance.)

To verify that the ultrahigh performance of the GbSB holds for problems other than K_{2000} , we also solved randomly generated 100 instances of the 700-spin Ising problem with all-to-all connectivity ($J_{i,j} \in \{\pm 1\}$) [24, 30] and the first ten instances of the well-known MAX-CUT benchmark set called G-set [8, 18–20, 24, 29, 31, 33–35, 48], which are equivalent to the 800-spin Ising problem with sparse connectivity ($J_{i,j} \in \{0, -1\}$ or $\{0, \pm 1\}$, see Fig. 2). Similarly to the case of K_{2000} , we obtained success probabilities exceeding 90% for 32 instances of the 700-spin problem and two G-set instances (G3 and G6). (See Tables I and II for the detailed results and settings.) Figures 1(b)(c) show the corresponding results of two of them to Fig. 1(a). Thus, the ultrahigh performance of the GbSB holds not only for K_{2000} but also for other large-scale problems.

IV. EDGE-OF-CHAOS EFFECT IN THE GBSB

To examine the reason for the ultrahigh performance of the GbSB, we investigated chaos in the GbSB as follows. We run the GbSB with two sets of initial conditions: $x_i^{(1)}(0) = \pm 0.1$ (\pm is randomly chosen) and $y_i^{(1)}(0) = 0$; $x_i^{(2)}(0) = x_i^{(1)}(0) \pm 2 \times 10^{-6}$ (\pm is randomly chosen) and $y_i^{(2)}(0) = 0$. Note that the two trajectories are very close to each other at the initial time. Next, we introduce the normalized distance $\delta(t)$ between the two trajectories as

$$\delta(t_m) = \sqrt{\frac{1}{4N} \sum_{i=1}^N [x_i^{(1)}(t_m) - x_i^{(2)}(t_m)]^2}. \quad (8)$$

From the above initial conditions, $\delta(0) = 10^{-6}$. Also note that $\delta \leq 1$ from $|x_i^{(1)}| \leq 1$ and $|x_i^{(2)}| \leq 1$, and the equality holds when $|x_i^{(1)} - x_i^{(2)}| = 2$ for all i . Most importantly, $\delta(t) \simeq 1/\sqrt{2}$ when all $x_i^{(1)}$ and $x_i^{(2)}$ become ± 1 randomly. That is, $\delta(t) \simeq 1/\sqrt{2}$ indicates the chaos.

The lower figures in Figs. 1(d-f) show the results of $\delta(t_M)$ (δ at the final time) corresponding to Figs. 1(a-c), respectively. In all the three cases, $\delta(t_M) \simeq 0$ when $A = 0$, indicating regular dynamics, and $\delta(t_M)$ converges to $1/\sqrt{2}$ (dotted lines) as A increases, indicating the chaos due to the nonlinear control. The regions highlighted in blue in Figs. 1(d-f) show the condition that the success probabilities become particularly high, as shown in the upper figures. We thus find that the success probabilities become high near the edge of chaos (between regular and chaotic regions). This result suggests that weakly chaotic processes occurring near regular dynamics may assist avoiding trapping at local minima and finding optimal solutions in the GbSB. This chaos-assisted solution search may be essentially different from conventional approaches with random noises such as SA, because the dramatic increase of the success probabilities, in particular, almost 100% success probabilities for the large-scale problems, has not been achieved by SA.

V. NO INFLUENCE OF DISCRETIZATION

We also investigated the dependence of the performance on the time step Δ_t . The results in Figs. 1(g-i) show that the notable behavior of the GbSB is independent of Δ_t . This result suggests that the high performance of the GbSB harnessing the edge of chaos comes not from artifacts due to the discretization for numerical simulations, but from the original Hamiltonian equations of motion with the walls and the nonlinear control of individual bifurcation parameters.

Figures 1(g-i) also show that P_S does not monotonically increase with respect to the number of steps M , unlike SA. To investigate the reason for this, we checked the normalized distance at the final time $\delta(t_M)$ corresponding to Figs. 1(g-i), the results of which are shown in Figs. 1(j-l). Interestingly, Fig. 1(j) suggests that P_S increases around the “valley of chaos.” This is also the case in Figs. 1(k) and 1(l), though they are less clear. This is natural in the sense that the butterfly effect becomes more evident for longer time evolution. Thus, a too large M (more precisely t_M) may result in chaos and consequently P_S may become lower.

VI. GBSB-BASED MACHINE WITH AN FPGA

To demonstrate high parallelizability of the GbSB, we designed a highly parallel custom circuit for the GbSB to minimize the execution time and then instantiated a 2,048-spin GbSB machine (GbSBM) with an FPGA

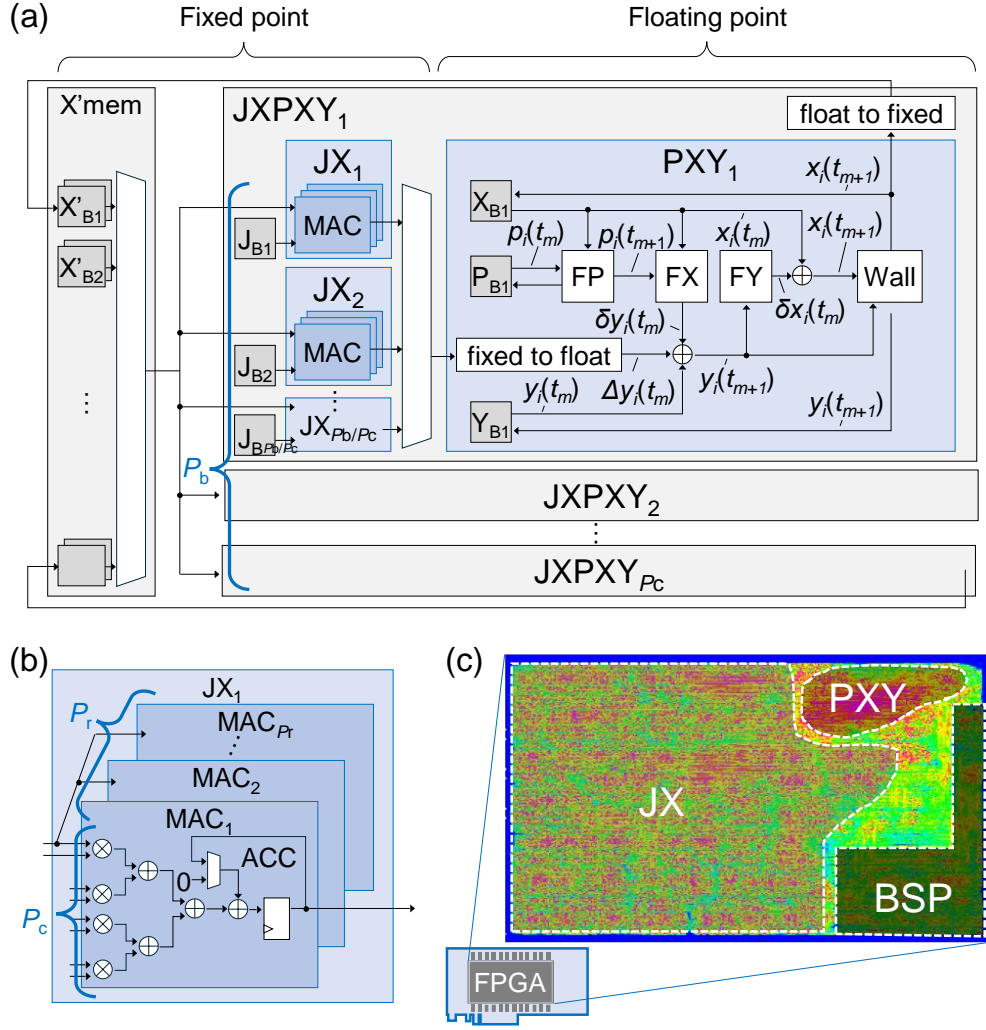


FIG. 2. GbSB-based machine with an FPGA. (a) Block diagram of the GbSB-based machine, which has a circulative structure corresponding to iteration of updating position and momentum: $y_i(t_{m+1}) = y_i(t_m) + \delta y_i(t_m) + \Delta y_i(t_m)$ and $x_i(t_{m+1}) = x_i(t_m) + \delta x_i(t_m)$, where $\Delta y_i(t_m) = JX[J_i, \mathbf{x}(t_m)] = c\Delta t \sum_{j=1}^N J_{i,j}x_j(t_m)$, $p_i(t_{m+1}) = FP[p_i(t_m), x_i(t_m)] = p_i(t_m) - [1 - Ax_i(t_m)^2]p_i(t_m)/(M - m)$, $\delta y_i(t_m) = FX[p_i(t_{m+1}), x_i(t_m)] = -p_i(t_{m+1})x_i(t_m)\Delta t$, and $\delta x_i(t_m) = FY[y_i(t_{m+1})] = y_i(t_{m+1})\Delta t$. The JX, FP, FX, FY modules in the block diagram correspond to the JX, FP, FX, FY functions, and the wall module executes the following conditional operation: $(x_i(t_{m+1}), y_i(t_{m+1})) \leftarrow \begin{cases} (\text{sgn}(x_i(t_{m+1})), 0), & \text{if } |x_i(t_{m+1})| > 1 \\ (x_i(t_{m+1}), y_i(t_{m+1})), & \text{otherwise} \end{cases}$. The computational precision of the JX module is 16-bit fixed point, while that for the remaining modules is 32-bit floating point. (b) Block diagram of a many-body interaction (JX) module. The parallelization parameters (P_r , P_c , and P_b) are illustrated in **a** and **b**. (c) Layout of the circuit modules in the FPGA, where the routing congestion is shown as a heatmap with the regions for the JX, PXY, and BSP (board support package) modules being indicated by dashed lines.

(Fig. 2). Each individual bifurcation parameter $p_i(t)$ newly introduced in the GbSB is updated depending only on its corresponding position $x_i(t)$ without depending on the other oscillators. Hence, the GbSB is highly parallelizable, as conventional SBs are [22–26]. The increase in computational complexity resulting from introducing individual parameters $p_i(t)$ [Eq. (7)] instead of a common parameter $p(t)$ [Eq. (6)] is $\Theta(N)$. In the computation for a GbSB time-evolution step, the many-body interaction computation, $\sum_{j=1}^N J_{i,j}x_j(t_m)$, in Eq. (3) is the most computationally intensive with a computational

complexity of $\Theta(N^2)$, while the remaining parts including updating $p_i(t)$, $x_i(t)$, and $y_i(t)$, collectively referred to as PXY, have a computational complexity of $\Theta(N)$. We accelerate the many-body interaction computation by spatial parallelization [referred to as JX in Fig. 2(a)], which is characterized by three parallelization parameters of P_r , P_c , and P_b [Figs. 2(a)(b)]. The PXY part is accelerated by temporal parallelization [Fig. 2(a)]. The number of the clock cycles per GbSB time-evolution step

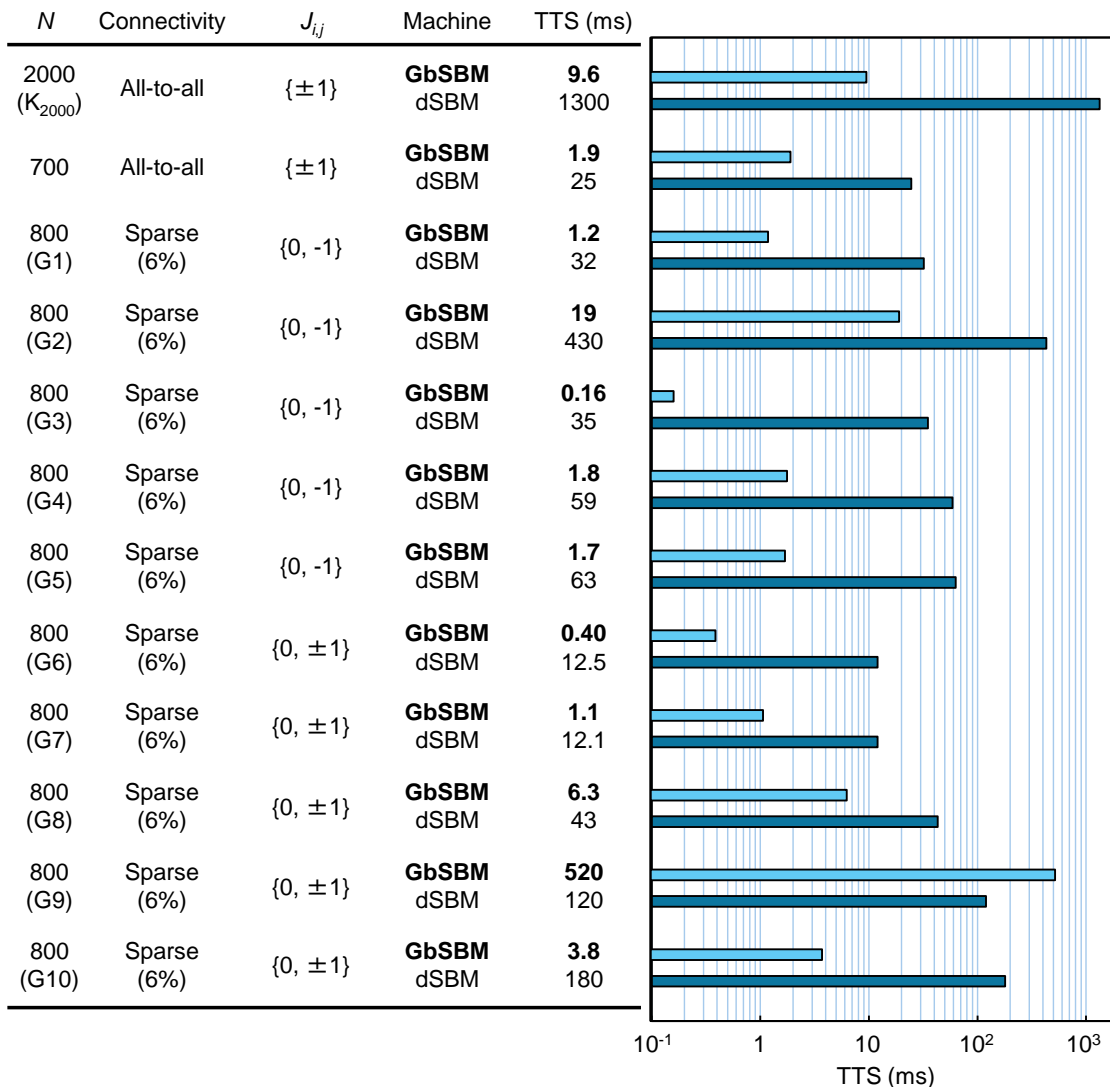


FIG. 3. Times to solution (TTSs) with a GbSB-based FPGA machine. The second row ($N = 700$) is the median of the TTSs for 100 random instances of the 700-spin Ising problem. See Appendix A for the detailed parameter settings and the GbSB-based machine (GbSBM). The results with the dSB-based machine (dSBM) are cited from ref. 24.

is expressed as

$$N_{\text{cyc}} = \frac{N^2}{P_r P_c P_b} + \frac{P_b P_r}{P_c} + \lambda, \quad (9)$$

where λ is the maximum circuit latency for circulative paths (See Appendix C for details). The circuit architecture accelerates the many-body interaction computation by $P_r P_c P_b$ and allows that $P_r P_c P_b$ can be larger than the number of oscillators N .

Dynamical system-based algorithms for combinatorial optimization often require complex functions, such as trigonometric functions [33] and hyperbolic tangent [4, 5, 32] (or other nonlinear functions [29]), and also pseudorandom number generators [20, 32]. Such functions consume a lot of computation resources when implemented with FPGAs. Unlike those, the GbSB is based

on only simple computations such as addition and multiplication, enabling a massively parallel implementation fully utilizing the capability of FPGAs. Figure 2(c) shows the circuit layout of the GbSBM ($N = 2,048$) in an FPGA. The computation parallelism, the number of multiply accumulation (MAC) processing elements for many-body interaction computation, achieved in this work is $P_r P_c P_b = 32,768$, where P_r , P_c , and P_b are 8, 32, and 128, respectively, leading to N_{cyc} of 260 clock cycles (λ is 100 clock cycles). We fully utilized the computing resources of the FPGA (the utilization of logic elements is 94%) and concurrently achieved almost the highest system clock frequency achievable with the FPGA ($F_{\text{sys}} = 591$ MHz). Consequently, the time per GbSB time-evolution step is $0.440 \mu\text{s}$. See Table III for details.

The GbSBM is evaluated in terms of times to so-

lution (TTSs) for the above problems. The TTS is defined as the computation time required for finding an optimal or best known solution with 99% probability. Mathematically, the TTS is formulated as $T_{\text{com}} \log(1 - 0.99) / \log(1 - P_S)$, where T_{com} is the computation time of a single run and if $P_S > 0.99$, the TTS is defined by T_{com} . The statistical error of the TTS, Δ_{TTS} , is given by $\Delta_{\text{TTS}} = \text{TTS} \times \Delta P_S / [(1 - P_S) |\ln(1 - P_S)|]$, where ΔP_S is the statistical error of P_S and formulated as $\Delta P_S = \sqrt{(P_S - P_S^2) / N_{\text{rep}}}$ (N_{rep} is the number of repetitions for estimating P_S) [24]. The 2,048-spin GbSBM can solve the 700-spin instances and the 800-spin G-set instances twice at the same time [24]. We did such a batch processing for these instances (the batch number is denoted by N_{batch}) and chose a better result, which enhances P_S while keeping the same T_{com} .

The results of the TTSs are summarized and compared with those obtained by a previously developed FPGA-based dSB machine (dSBM) [24] in Fig. 3, where dSB is obtained from bSB by replacing $J_{i,j} x_j(t_m)$ with $J_{i,j} s_j(t_m)$ in Eq. (3). First, the TTS for K_{2000} is shortened to 9.6 ms by the GbSBM from 1.3 s of the dSBM, leading to two orders of magnitude improvement. Similarly, the median of the TTSs for the 100 instances of the 700-spin Ising problem and the TTSs for the G-set instances are one or two orders of magnitude shortened except for G9. These results support the expectation that the GbSB harnessing the edge of chaos will substantially enhance the performance of SB-based machines.

VII. SUMMARY AND OUTLOOK

We have generalized bSB by introducing nonlinear control of individual bifurcation parameters such that the oscillators in the bSB do not stick to walls. We have found that the success probabilities of the generalized bSB (GbSB) for large-scale problems dramatically increase and sometimes approach almost 100%. Developing a GbSB-based machine with an FPGA, we have demonstrated one or two orders of magnitude improvements of times to solution for the large-scale problems compared with a previously developed SB-based FPGA machine. By investigating chaos in the GbSB, we have also found that the surprising increase of the success probabilities occurs near the edge of chaos. This result suggests that the GbSB can achieve the ultrahigh performance by harnessing the edge of chaos. The present study on chaos is based on numerical experiments. Theoretical studies on the present system are desirable but left for future work. Also, the above conclusion is based on numerical study on 111 specific instances, and therefore investigating more instances from a wider range of problem classes is also desirable.

Our results open broad and interesting possibilities as follows. In this work, we have focused on bSB and found the edge-of-chaos effect. It is thus interesting whether or not other dynamical-system approaches, such

as aSB [22], dSB [24], neural networks [4, 5], coherent Ising machines [6–11], and oscillator-based Ising machines [33, 34], exhibit similar effects by similar nonlinear control. The GbSB has an additional parameter, namely, the nonlinear-control strength, which requires additional tuning for achieving high performance, together with tuning of the number of time steps. Although we have not included the time to optimize these parameters in computation times in this work, as in previous studies, the optimization time is not negligible for practical applications. To optimize the parameters quickly, our finding that good parameter values may be found around the edge of chaos will be helpful. The GbSB could not improve G9, one of the G-set instances, compared with dSB. This result suggests the limitation of the power of GbSB. While it is important to clarify the range of applicability of GbSB, this result suggests that we may need a hybrid algorithm combining GbSB with others for solving a wide range of problems. In general, the SBs can achieve high performance for dense-connectivity problems [3, 69]. On the other hand, a dynamical-system approach that can achieve ultrahigh performance for sparse-connectivity problems has recently been reported [70]. The combination of them will be promising to tackle both kinds of problems.

ACKNOWLEDGEMENTS

RH and KT thank Masaya Yamasaki for his kind help.

Appendix A: Parameter settings in the GbSB

The GbSB has two parameters: a time step Δ_t and a constant c for tuning the first bifurcation point, similarly to the other SB algorithms [22–28]. In this work, we set them as follows. In the cases of conventional SB algorithms with a single bifurcation parameter $p(t)$, the first bifurcation point is given by $p(t) = c\lambda_{\text{max}}$, where λ_{max} is the largest eigenvalue of the interaction matrix J [22, 24]. λ_{max} is positive because the trace of J is zero. To set the first bifurcation point at the initial time for eliminating useless dynamics before the bifurcation, c is usually set as $c = p(0) / \lambda_{\text{max}} = 1 / \lambda_{\text{max}}$ [22, 24]. Similarly, we set $c = 1 / \lambda_{\text{max}}$ in the GbSB because $p_i(0) = 1$. Note that we can estimate λ_{max} for a random matrix, such as that of K_{2000} , as $\lambda_{\text{max}} = 2\sqrt{N}\sigma$ from Wigner’s semicircle law, where σ is the standard deviation of the nondiagonal elements of J . In this work, we thus set $c = 1 / (2\sqrt{N}\sigma) = 1 / (2\sqrt{N})$ for K_{2000} and the 100 instances of the 700-spin Ising problem. For the ten instances of G-set, we numerically evaluate λ_{max} and set $c = 1 / \lambda_{\text{max}}$.

For the setting of Δ_t , we consider the stability condition for the Hamiltonian dynamics. At the initial time, the Hamiltonian system is equivalent to the system of N harmonic oscillators with mass of unity and spring constants of $k_i = p(0) - c\lambda_i = 1 - \lambda_i / \lambda_{\text{max}}$, where λ_i is the

i th eigenvalue of J . The position and momentum of the i th harmonic oscillator are denoted by x_i and y_i , respectively. Then, from the update rules of the symplectic Euler method [52] in Eqs. (3) and (4), we have $y_i(t_{m+1}) = y_i(t_m) - k_i x_i(t_m) \Delta_t$ and $x_i(t_{m+1}) = x(t_m) + y_i(t_{m+1}) \Delta_t$, which result in

$$x_i(t_{m+1}) - (2 - k_i \Delta_t^2) x_i(t_m) + x_i(t_{m-1}) = 0. \quad (\text{A1})$$

The condition that Eq. (A1) describes oscillation is given by $(2 - k_i \Delta_t^2)^2 - 4 < 0$, leading to the following stability condition for the i th harmonic oscillator:

$$\Delta_t < \frac{2}{\sqrt{k_i}} = \frac{2}{\sqrt{1 - \lambda_i/\lambda_{\max}}}. \quad (\text{A2})$$

Thus, the sufficient condition for Δ_t satisfying Eq. (A2) for all the harmonic oscillators is given by

$$\Delta_t < \frac{2}{\sqrt{1 - \lambda_{\min}/\lambda_{\max}}}, \quad (\text{A3})$$

where λ_{\min} is the minimum eigenvalue of J . Note that λ_{\min} is negative, because the trace of J is zero, and can be estimated as $\lambda_{\min} = -2\sqrt{N}\sigma$ for a random matrix. In the case of a random matrix, Eq. (A3) is reduced to $\Delta_t < \sqrt{2} = 1.414 \dots$. This is the reason why $\Delta_t = 1.25$ resulted in good performance for K_{2000} and other random instances in the previous study [24]. In this work, we also used $\Delta_t = 1.25$ for K_{2000} and the 100 instances of the 700-spin Ising problem. We can generalize this setting to the general case by using Eq. (A3) as follows:

$$\Delta_t = D_t \sqrt{\frac{2}{1 - \lambda_{\min}/\lambda_{\max}}} \quad (\text{A4})$$

with $D_t = 1.25$. We used this setting of Δ_t for the ten instances of G-set in this work.

As for initial conditions, $x_i(0)$ was set to a random value between -1 and 1 , except the simulations to evaluate $\delta(t_M)$ in Figs. 1(d-f), and $y_i(0)$ was set to zero.

Appendix B: Average cut values in Figs. 1(a-c)

Figures 1(a-c) show the success probability P_S to obtain the best known value, where $P_S \simeq 0$ in a wide range of the parameters. Here we show the average cut value C_{ave} normalized by the best known value C_{best} in Fig. 4. We can confirm the gradual improvement of C_{ave} by GbSB.

Appendix C: FPGA implementation of GbSB

Figure 5(a) shows the timing chart of the operation of JX and PXY modules. As shown in Fig. 5(b), a JX module processes $P_r P_c$ multiply-accumulation operations per clock cycle and then produce P_r numbers of Δy_i after

N/P_c cycles (hereafter, a phase), and there are P_b JX modules. A PXY module shown in Fig. 2a takes as input a Δy_i datum per clock cycle and processes $P_b P_r / P_c$ numbers of Δy_i data per phase, and there are P_c PXY modules. The operation of a PXY module is overlapped with that of JX modules in time domain [Fig. 5(a)]. The maximum circuit latency for circulative paths is denoted by λ , meaning that the system must wait for λ to guarantee that the final datum has been stored in memory after the final iteration begins. Thus, the number of the clock cycles per GbSB time-evolution step, N_{cyc} , is expressed by Eq. (9).

Table III summarizes the details of implementation and performance of the FPGA-based GbSB machine. The computational precision of the PXY module is 32-bit floating point, while that of the JX module uses less precision, i.e., 16-bit fixed point, to increase the parallelism of JX modules. The FPGA board used in this work (Bittware IA-840F Intel Agilex FPGA card) is equipped with an Intel Agilex7F AGF027 FPGA. The design is described and synthesized using Quartus Prime Pro 21.4 CAD tool. The limiting resource to determine the achievable maximum parallelism is logic elements used to synthesize JX modules. The system clock frequency F_{sys} determined as a result of circuit synthesis, placement, and routing is 591 MHz, corresponding to clock cycle time T_{cycle} of 1.69 ns. The maximum circuit latency for circulative paths, λ , is 100 clock cycles.

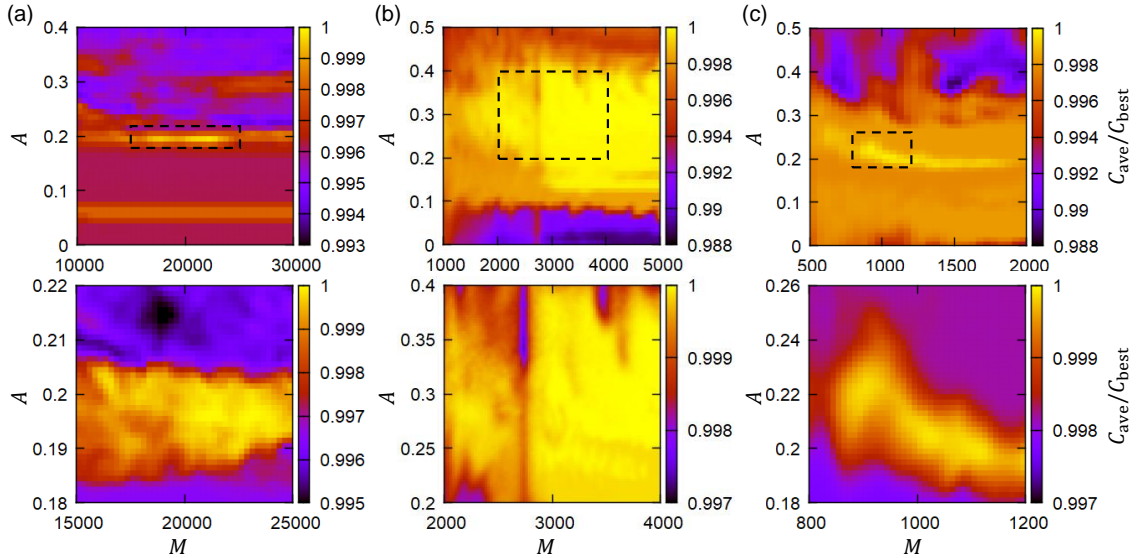


FIG. 4. Average cut value C_{ave} normalized by the best know value C_{best} corresponding to Figs. 1(a–c), respectively.

TABLE I. Detailed results and settings for K2000 and the first ten instances of G-set. Δ_{TTS} and ΔP_S are the standard errors of TTS and P_S , respectively. They can be simply formulated as $\Delta P_S = \sqrt{(P_S - P_S^2)/N_{\text{rep}}}$ and $\Delta_{\text{TTS}} = \text{TTS} \times \Delta P_S / [(1 - P_S) \ln(1 - P_S)]$, where N_{rep} is the number of repetitions for their evaluation [24].

Instance	TTS (ms)	Δ_{TTS} (ms)	P_S (%)	ΔP_S (%)	M	A	N_{rep}	N_{batch}
K ₂₀₀₀	9.61	1.47	98.9	0.3	21400	0.196	1000	1
G1	1.20	0.14	39.7	1.5	300	0.5	1000	2
G2	19.23	1.66	7.1	0.3	700	0.48	10000	2
G3	0.16	0.02	98.7	0.4	350	0.04	1000	2
G4	1.80	0.21	39.8	1.5	450	0.61	1000	2
G5	1.72	0.16	69.3	1.5	1000	0.41	1000	2
G6	0.40	0.07	99.3	0.3	900	0.22	1000	2
G7	1.08	0.10	77.7	1.3	800	0.35	1000	2
G8	6.32	1.20	14.8	1.1	500	0.28	1000	2
G9	519.03	95.69	0.16	0.01	400	0.53	100000	2
G10	3.77	0.86	10.2	1.0	200	0.57	1000	2

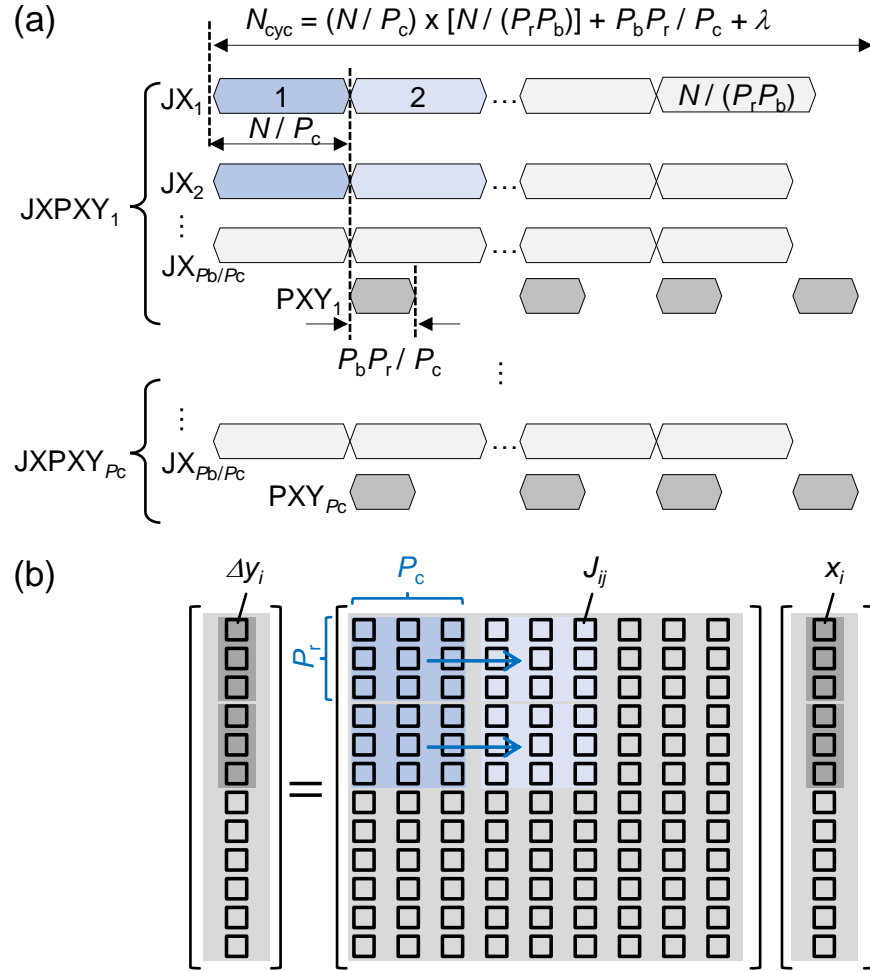


FIG. 5. Parallel processing of the computation in a GbSB time-evolution step. (a) Timing chart of the operation of JX and PXY modules. (b) A schematic showing how the many-body interaction computations, $\sum_{j=1}^N J_{i,j} x_j(t_m)$, are processed in parallel.

TABLE II. Detailed results and settings in the ascending order of TTSs for the 100 instances of the 700-spin Ising problem. The instance in Fig. 1 is highlighted in bold. Δ_{TTS} and ΔP_S are the standard errors of TTS and P_S , respectively (see the caption of Table I for their definitions).

TTS (ms)	Δ_{TTS} (ms)	P_S (%)	ΔP_S (%)	M	A	N_{rep}	N_{batch}
0.09	0.03	99.0	0.7	200	0	200	2
0.11	0.04	99.0	0.7	250	0.17	200	2
0.11	0.05	99.5	0.5	250	0.36	200	2
0.12	0.03	97.0	1.2	200	0.1	200	2
0.12	0.04	98.5	0.9	250	0.4	200	2
0.13	0.05	99.0	0.7	300	0.02	200	2
0.14	0.05	98.5	0.9	300	0.01	200	2
0.15	0.07	99.5	0.5	350	0.17	200	2
0.20	0.09	99.5	0.5	450	0.04	200	2
0.20	0.07	99.0	0.7	450	0.17	200	2
0.22	0.07	98.5	0.9	450	0.31	200	2
0.22	0.06	97.5	1.1	400	0	200	2
0.22	0.10	99.5	0.5	500	0.04	200	2
0.23	0.05	82.5	2.7	200	0.05	200	2
0.25	0.05	91.0	2.0	300	0	200	2
0.26	0.08	98.0	1.0	500	0.09	200	2
0.30	0.06	63.5	3.4	150	0.17	200	2
0.31	0.07	63.0	3.4	150	0	200	2
0.31	0.11	99.0	0.7	700	0.15	200	2
0.31	0.11	99.0	0.7	700	0.3	200	2
0.31	0.00	100	0	700	0	200	2
0.33	0.07	84.5	2.6	300	0	200	2
0.35	0.00	100	0	800	0.07	200	2
0.35	0.15	99.5	0.5	800	0.34	200	2
0.39	0.08	65.0	3.4	200	0.38	200	2
0.40	0.14	99.0	0.7	900	0.02	200	2
0.40	0.14	99.0	0.7	900	0	200	2
0.44	0.09	87.5	2.3	450	0.29	200	2
0.44	0.09	68.5	3.3	250	0.34	200	2
0.44	0.19	99.5	0.5	1000	0.18	200	2
0.44	0.00	100	0	1000	0	200	2
0.60	0.15	96.5	1.3	1000	0	200	2
0.60	0.15	96.5	1.3	1000	0.05	200	2
0.66	0.13	78.5	2.9	500	0.31	200	2
0.66	0.00	100	0	1500	0.26	200	2
0.69	0.15	90.5	2.1	800	0.47	200	2
0.72	0.15	86.0	2.5	700	0.31	200	2
0.78	0.23	98.0	1.0	1500	0.43	200	2
0.78	0.17	92.5	1.9	1000	0.28	200	2
0.86	0.19	61.0	3.4	400	0.31	200	2
0.89	0.18	74.5	3.1	600	0.38	200	2
1.16	0.18	23.1	1.3	150	0.29	1000	2
1.29	0.21	21.0	1.3	150	0.26	1000	2
1.32	0.57	99.5	0.5	3000	0.25	200	2
1.35	0.28	70.0	3.2	800	0.49	200	2
1.64	0.29	16.9	1.2	150	0.21	1000	2
1.69	0.40	95.0	1.5	2500	0.23	200	2
1.73	0.44	41.0	3.5	450	0.31	200	2
1.76	0.37	64.5	3.4	900	0.28	200	2
1.89	0.38	80.0	2.8	1500	0.2	200	2

TTS (ms)	ΔTTS (ms)	P_S (%)	ΔP_S (%)	M	A	N_{rep}	N_{batch}
1.97	0.30	22.7	1.3	250	0.35	1000	2
2.30	0.59	41.0	3.5	600	0.4	200	2
2.39	0.67	34.5	3.4	500	0.46	200	2
2.69	0.69	41.0	3.5	700	0.37	200	2
2.85	0.44	22.0	1.3	350	0.21	1000	2
3.20	0.68	11.9	1.0	200	0	1000	2
3.37	0.60	16.5	1.2	300	0.36	1000	2
3.41	0.96	34.0	3.3	700	0.38	200	2
3.50	0.48	5.62	0.33	100	0.09	5000	2
3.83	1.07	34.5	3.4	800	0.56	200	2
4.02	0.57	26.1	1.4	600	0.53	1000	2
4.15	0.62	4.76	0.30	100	0.05	5000	2
4.35	0.95	11.0	1.0	250	0.52	1000	2
4.67	0.91	14.1	1.1	350	0.47	1000	2
4.93	1.05	11.6	1.0	300	0.49	1000	2
4.95	0.52	9.72	0.42	250	0.33	5000	2
5.08	0.71	27.3	1.4	800	0.24	1000	2
5.18	1.05	12.8	1.1	350	0.59	1000	2
5.45	0.76	5.42	0.32	150	0.57	5000	2
5.85	0.61	50.0	1.6	2000	0.49	1000	2
6.01	1.11	15.5	1.1	500	0.46	1000	2
6.76	0.82	7.22	0.37	250	0.32	5000	2
7.00	0.79	8.32	0.39	300	0.43	5000	2
7.35	1.45	2.72	0.23	100	0	5000	2
7.41	1.75	49.5	3.5	2500	0.45	200	2
8.96	1.39	4.42	0.29	200	0.42	5000	2
9.22	1.45	4.30	0.29	200	0.59	5000	2
11.18	1.48	30.4	1.5	2000	0.22	1000	2
11.68	1.78	22.9	1.3	1500	0.63	1000	2
12.10	2.16	1.66	0.13	100	0.05	10000	2
12.21	1.57	6.42	0.35	400	0.32	5000	2
15.62	2.03	6.28	0.34	500	0.41	5000	2
16.40	3.42	2.44	0.22	200	0.47	5000	2
18.48	4.08	1.09	0.10	100	0.03	10000	2
19.38	2.56	6.08	0.34	600	0.61	5000	2
20.14	2.52	6.80	0.36	700	0.62	5000	2
22.56	4.63	12.6	1.0	1500	0.46	1000	2
23.22	4.69	1.30	0.11	150	0.37	10000	2
26.26	5.06	14.3	1.1	2000	0.62	1000	2
28.94	6.06	2.42	0.22	350	0.44	5000	2
30.26	6.04	1.33	0.11	200	0.21	10000	2
30.70	1.56	20.6	0.4	3500	0.51	10000	2
31.59	5.51	17.5	1.2	3000	0.51	1000	2
35.81	4.97	5.50	0.32	1000	0.42	5000	2
112.09	20.28	0.81	0.06	450	0.66	20000	2
112.99	25.15	1.07	0.10	600	0.55	10000	2
116.90	20.46	0.35	0.03	200	0.34	50000	2
175.15	28.38	0.40	0.03	350	0.26	50000	2
208.30	38.53	0.78	0.06	800	0.43	20000	2
374.24	55.28	0.49	0.03	900	0.59	50000	2

TABLE III. Implementation and performance of the GbSB-based FPGA machine.

Architecture		
Machine size N (# of spins)	2,048	
Computational precision	Mixed (16-bit fixed & 32-bit floating)	
Parallelism: P_r, P_c, P_b	8, 32, 128	
# of processing elements (MACs)	32,768	
Resource usage		
	Usage	Resource
Logic elements [count]	860,354 (94%)	912,800
RAM blocks [count]	3,286 (25%)	13,272
DSP blocks [count]	436 (5%)	8,528
Performance		
F_{sys} [MHz]	591	
T_{cycle} [ns]	1.69	
Latency λ [cycle]	100	
Clock cycles per GbSB step [cycle]	260	
Time per GbSB step [μs]	0.440	

- [1] P. Siarry, *Metaheuristics* (Springer International Publishing, 2016).
- [2] G. Finocchio et al., *Roadmap for unconventional computing with nanotechnology*, Nano Futures **8**, 012001 (2024).
- [3] N. Mohseni, P. L. McMahon, and T. Byrnes, *Ising machines as hardware solvers of combinatorial optimization problems*, Nat. Rev. Phys. **4**, 363 (2022).
- [4] J. J. Hopfield and D. W. Tank, “*Neural*” computation of decisions in optimization problems, Biol. Cybern. **52**, 141 (1985).
- [5] J. J. Hopfield and D. W. Tank, *Computing with neural circuits: a model*, Science **233**, 625 (1986).
- [6] Z. Wang, A. Marandi, K. Wen, R. L. Byer, and Y. Yamamoto, *Coherent Ising machine based on degenerate optical parametric oscillators*, Phys. Rev. A **88**, 063853 (2013).
- [7] A. Marandi, Z. Wang, K. Takata, R. L. Byer, and Y. Yamamoto, *Network of time-multiplexed optical parametric oscillators as a coherent Ising machine*, Nat. Photon. **8**, 937 (2014).
- [8] T. Inagaki et al., *A coherent Ising machine for 2000-node optimization problems*, Science **354**, 603 (2016).
- [9] P. L. McMahon et al., *A fully programmable 100-spin coherent Ising machine with all-to-all connections*, Science **354**, 614 (2016).
- [10] Y. Yamamoto, K. Aihara, T. Leleu, K.-I. Kawarabayashi, S. Kako, M. Fejer, K. Inoue, and H. Takesue, *Coherent Ising machines—Optical neural networks operating at the quantum limit*, npj Quantum Inf. **3**, 49 (2017).
- [11] T. Honjo et al., *100,000-spin coherent Ising machine*, Sci. Adv. **7**, eabh0952 (2021).
- [12] H. Goto, *Bifurcation-based adiabatic quantum computation with a nonlinear oscillator network*, Sci. Rep. **6**, 21686 (2016).
- [13] S. Puri, C. K. Andersen, A. L. Grimsmo, and A. Blais, *Quantum annealing with all-to-all connected nonlinear oscillators*, Nat. Commun. **8**, 15785 (2017).
- [14] H. Goto, Z. Lin, and Y. Nakamura, *Boltzmann sampling from the Ising model using quantum heating of coupled nonlinear oscillators*, Sci. Rep. **8**, 7154 (2018).
- [15] H. Goto, *Quantum computation based on quantum adiabatic bifurcations of Kerr-nonlinear parametric oscillators*, J. Physical Soc. Japan **88**, 061015 (2019).
- [16] H. Goto and T. Kanao, *Quantum annealing using vacuum states as effective excited states of driven systems*, Commun. Phys. **3**, 235 (2020).
- [17] T. Kanao and H. Goto, *High-accuracy Ising machine using Kerr-nonlinear parametric oscillators with local four-body interactions*, npj Quant. Inf. **7**, 18 (2021).
- [18] K. P. Kalinin and N. G. Berloff, *Global optimization of spin Hamiltonians with gain-dissipative system*, Sci. Rep. **8**, 17791 (2018).
- [19] T. Leleu, Y. Yamamoto, P. L. McMahon, and K. Aihara, *Destabilization of local minima in analog spin systems by correction of amplitude heterogeneity*, Phys. Rev. Lett. **122**, 040607 (2019).
- [20] E. S. Tiunov, A. E. Ulanov, and A. I. Lvovsky, *Annealing by simulating the coherent Ising machine*, Opt. Exp. **27**, 10288 (2019).
- [21] F. Sheldon, F. L. Traversa, and M. Di Ventra, *Taming a nonconvex landscape with dynamical long-range order: Memcomputing Ising benchmarks*, Phys. Rev. E **100**, 053311 (2019).
- [22] H. Goto, K. Tatsumura, and A. R. Dixon, *Combinatorial optimization by simulating adiabatic bifurcations in nonlinear Hamiltonian systems*, Sci. Adv. **5**, eaav2372 (2019).
- [23] K. Tatsumura, A. R. Dixon, and H. Goto, *FPGA-based simulated bifurcation machine*, in Proceedings of IEEE Int’l Conference on Field-Programmable Logic and Applications (FPL) (2019), pp. 59–66.
- [24] H. Goto et al., *High-performance combinatorial optimization based on classical mechanics*, Sci. Adv. **7**, eabe7953 (2021).
- [25] K. Tatsumura, M. Yamasaki, and H. Goto, *Scaling out Ising machines using a multi-chip architecture for simulated bifurcation*, Nat. Electron. **4**, 208 (2021).
- [26] T. Kashimata, M. Yamasaki, R. Hidaka, and K. Tatsumura, *Efficient and Scalable Architecture for Multiple-Chip Implementation of Simulated Bifurcation Machines*, IEEE Access **12**, 36606 (2024).
- [27] T. Kanao and H. Goto, *Simulated bifurcation assisted by thermal fluctuation*, Commun. Phys. **5**, 153 (2022).
- [28] T. Kanao and H. Goto, *Simulated bifurcation for higher-order cost functions*, Appl. Phys. Express **16**, 014501 (2023).
- [29] F. Böhm, T. Van Vaerenbergh, G. Verschaffelt, and G. Van der Sande, *Order-of-magnitude differences in computational performance of analog Ising machines induced by the choice of nonlinearity*, Commun. Phys. **4**, 149 (2021).
- [30] T. Leleu, F. Khoystatee, T. Levi, R. Hamerly, T. Kohno, and K. Aihara, *Scaling advantage of chaotic amplitude control for high-performance combinatorial optimization*, Commun. Phys. **4**, 266 (2021).
- [31] S. Reifenstein, S. Kako, F. Khoystatee, T. Leleu, and Y. Yamamoto, *Coherent Ising Machines with Optical Error Correction Circuits*, Adv. Quantum Technol. **4**, 2100077 (2021).
- [32] N. A. Aadit, A. Grimaldi, M. Carpentieri, L. Theogarajan, J. M. Martinis, G. Finocchio, and K. Camsari, *Massively parallel probabilistic computing with sparse Ising machines*, Nat. Electron. **5**, 460 (2022).
- [33] L. Mazza, E. Raimondo, A. Grimaldi, and V. Puliafito, *Simulated Oscillator-Based Ising Machine for Two Million Nodes Max-Cut Problems*, in 2023 IEEE 23rd International Conference on Nanotechnology (NANO) (IEEE, 2023), pp. 1037–1041.
- [34] M. S. Ansari, H. Nehete, A. Grimaldi, L. Mazza, E. Raimondo, V. Puliafito, G. Finocchio, and B. K. Kaushik, *A comparison of Oscillatory Ising Machines and Simulated Bifurcation Machines for Solving Maximum Cut Problems*, in 2024 IEEE 24th International Conference on Nanotechnology (NANO), Gijon, Spain, 2024, pp. 389–393.
- [35] M. Nakazawa and T. Hirooka, *An Oscillator-Less Photonic Ising Machine With Digital-Nonlinearity-Based Bifurcation and Its Simulated Application to a 1 Million-Node Fully Connected Max-Cut Problem*, J. Lightwave Technology **43**, 5579 (2025).
- [36] W.-A. Borders, A.-Z. Pervaiz, S. Fukami, K.-Y. Camsari, H. Ohno, and S. Datta, *Integer factorization using stochastic magnetic tunnel junctions*, Nature (London)

- 573**, 390 (2019).
- [37] F. Böhm, G. Verschaffelt, and G. Van der Sande, *A poor man's coherent Ising machine based on opto-electronic feedback systems for solving optimization problems*, Nat. Commun. **10**, 3538 (2019).
- [38] T. Wang and J. Roychowdhury, *OIM: Oscillator-Based Ising Machines for Solving Combinatorial Optimisation Problems*, in Lecture Notes in Computer Science (Including Subseries Lecture Notes in Artificial Intelligence and Lecture Notes in Bioinformatics), Vol. 11493 LNCS (Springer International Publishing, 2019), pp. 232–256.
- [39] K. P. Kalinin, A. Amo, J. Bloch, and N. G. Berloff, *Polaritonic XY-Ising machine*, Nanophotonics **9**, 4127 (2020).
- [40] F. Cai et al., *Power-efficient combinatorial optimization using intrinsic noise in memristor Hopfield neural networks*, Nat. Electron. **3**, 409 (2020).
- [41] T. Wang, L. Wu, P. Nobel, and J. Roychowdhury, *Solving Combinatorial Optimisation Problems Using Oscillator Based Ising Machines*, Nat. Comput. **20**, 287 (2021).
- [42] D. I. Albertsson, M. Zahedinejad, A. Houshang, R. Khymyn, J. øAkerman, and A. Rusu, *Ultrafast Ising Machines using spin torque nano-oscillators*, Appl. Phys. Lett. **118**, 112404 (2021).
- [43] R. Afoakwa, Y. Zhang, U. K. R. Vengalam, Z. Ignjatovic, and M. Huang, *BRIM: Bistable Resistively-Coupled Ising Machine*, in 2021 IEEE International Symposium on High-Performance Computer Architecture (HPCA), Seoul, Korea (South), pp. 749–760 (2021).
- [44] A. Sharma, R. Afoakwa, Z. Ignjatovic, and M. Huang, *Increasing Ising machine capacity with multi-chip architectures*, in Proc. of Annual International Symposium on Computer Architecture (ISCA), pp. 508–521 (2022).
- [45] W. Moy, I. Ahmed, P. Chiu, J. Moy, S. S. Sapatnekar, and C. H. Kim, *A 1,968-node coupled ring oscillator circuit for combinatorial optimization problem solving*, Nat. Electron. **5**, 310 (2022).
- [46] A. Grimaldi et al., *A 1,968-node coupled ring oscillator circuit for combinatorial optimization problem solving*, Evaluating Spintronics-Compatible Implementations of Ising Machines, Phys. Rev. Appl. **20**, 024005 (2023).
- [47] M. Graber and K. Hofmann, *A 1,968-node coupled ring oscillator circuit for combinatorial optimization problem solving*, An integrated coupled oscillator network to solve optimization problems, Commun. Eng. **3**, 116 (2024).
- [48] K. P., Kalinin et al., *Analog optical computer for AI inference and combinatorial optimization*, Nature (London) **645**, 354 (2025).
- [49] H. Goto, *Universal quantum computation with a nonlinear oscillator network*, Phys. Rev. A **93**, 050301(R) (2016).
- [50] S. Puri, S. Boutin, and S., A. Blais, *Engineering the quantum states of light in a Kerr-nonlinear resonator by two-photon driving*, npj Quantum Inf. **3**, 18 (2017).
- [51] S. Arora and B. Barak, *Computational Complexity: A Modern Approach* (Cambridge Univ. Press, 2009).
- [52] B. Leimkuhler and S. Reich, *Simulating Hamiltonian Dynamics* (Cambridge University Press, 2004).
- [53] L. D. Landau, and E. M. Lifshitz, *Mechanics* (Butterworth-Heinemann, Third Edition, 1976).
- [54] H. Goldstein, C. Poole, and J. Safko, *Classical Mechanics* (Addison Wesley, Third Edition, 2000).
- [55] S. Kirkpatrick, C. D. Gelatt Jr., and M. P. Vecchi, *Optimization by Simulated Annealing*, Science **220**, 671 (1983).
- [56] S. H. Strogatz, *Nonlinear dynamics and chaos* (Westview Press, Boulder, CO, Second Edition, 2015).
- [57] S. Wimberger, *Nonlinear Dynamics and Quantum Chaos* (Springer, Cham, 2014).
- [58] C. G. Langton, *Computation at the edge of chaos: Phase transitions and emergent computation*, Phys. D Nonlinear Phenomena **42**, 12 (1990).
- [59] N. Bertschinger and T. Natschläger, *Real-time computation at the edge of chaos in recurrent neural networks*, Neural Comput. **16**, 1413 (2004).
- [60] J. Boedecker, O. Obst, J. T. Lizier, N. M. Mayer, and M. Asada, *Information processing in echo state networks at the edge of chaos*, Theory Biosci. **131**, 205 (2012).
- [61] J. Hochstetter, R. Zhu, A. Loeffler, A. Diaz-Alvarez, T. Nakayama, and Z. Kuncic, *Avalanches and edge-of-chaos learning in neuromorphic nanowire networks*, Nat. Commun. **12**, 4008 (2021).
- [62] D. Nishioka et al., *Edge-of-chaos learning achieved by ion-electron-coupled dynamics in an ion-gating reservoir*, Sci. Adv. **8**, eade1156 (2022).
- [63] M. Yan, C. Huang, P. Bienstman, P. Tino, W. Lin, and J. Sun, *Emerging opportunities and challenges for the future of reservoir computing*, Nat. Commun. **15**, 2056 (2024).
- [64] M. Hasegawa, T. Ikeguchi, T. Matozaki, and K. Aihara, *Solving combinatorial optimization problems by nonlinear neural dynamics*, in Proceedings of ICNN'95 - International Conference on Neural Networks, Perth, WA, Australia, vol.6, pp. 3140-3145 (1995).
- [65] T. Ikeguchi, K. Sato, M. Hasegawa, and K. Aihara, *Chaotic optimization for quadratic assignment problems*, in 2002 IEEE International Symposium on Circuits and Systems (ISCAS), Phoenix-Scottsdale, AZ, USA, pp. III-III (2002).
- [66] Y. Tang, N. Zhang, P. Zhu, M. Fang, and G. He, *Application of the edge of chaos in combinatorial optimization*, Chin. Phys. B **30**, 100505 (2021).
- [67] F. Barahona, *On the computational complexity of Ising spin glass models*, J. Phys. A **15**, 3241 (1982).
- [68] A. Lucas, *Ising formulations of many NP problem*, Front. Phys. **2**, 5 (2014).
- [69] H. Oshiyama and M. Ohzeki, *Benchmark of quantum-inspired heuristic solvers for quadratic unconstrained binary optimization*, Sci. Rep. **12**, 2146 (2022).
- [70] K. M. Zick, *Performance report of heuristic algorithm that cracked the largest Gset Ising problems (G81 cut=14060)*, arXiv:2505.18508 [Computer Science] (2025).